Dynamic Modeling Accuracy Dependence on Errors in Sensor Measurements, Mass Properties, and Aircraft Geometry

Jared A. Grauer* and Eugene A. Morelli†
NASA Langley Research Center, Hampton, Virginia, 23681

A nonlinear simulation of the NASA Generic Transport Model was used to investigate the effects of errors in sensor measurements, mass properties, and aircraft geometry on the accuracy of dynamic models identified from flight data. Measurements from a typical system identification maneuver were systematically and progressively deteriorated and then used to estimate stability and control derivatives within a Monte Carlo analysis. Based on the results, recommendations were provided for maximum allowable errors in sensor measurements, mass properties, and aircraft geometry to achieve desired levels of dynamic modeling accuracy. Results using other flight conditions, parameter estimation methods, and a full-scale F-16 nonlinear aircraft simulation were compared with these recommendations.

Nomenclature

Roman

a	acceleration [ft/s^2]
b	wingspan [ft]
C	coefficient
$\bar{c}$	mean aerodynamic chord [ft]
$\mathbf{e}$	error vector
I	inertia [slug $\cdot$ ft^2]
$J(\boldsymbol{\theta})$	cost function
j	imaginary number, $\sqrt{-1}$
L, M, N	applied body torques [lbf $\cdot$ ft]
m	mass [slug]
p, q, r	body frame angular velocities [rad/s]
$\bar{q}$	dynamic pressure [lbf/ft^2]
$\Re$	real part
S	wing reference area [ft^2]
T	data record length [s]
t	time [s]
V	airspeed [ft/s]
$\mathbf{X}$	regressor matrix
X, Y, Z	applied body forces [lbf]
$\mathbf{z}$	measurement vector

Greek

α	angle of attack [rad]
β	sideslip angle [rad]
Δ	perturbation value
δ	control surface deflection [rad]
$\boldsymbol{\theta}$	parameter vector
ρ	air density [slug/ft^3]
$\boldsymbol{\Sigma}$	parameter covariance
ϕ, θ, ψ	Euler angles [rad]
ω	frequency [rad/s]

Superscripts

$\dot{}$	time derivative
$\dagger$	complex conjugate transpose
$\hat{}$	estimated value
$^{-1}$	inverse

Subscripts

$_0$	trim value
$_a$	aileron
$_e$	elevator
$_r$	rudder

*Research Engineer, Dynamic Systems and Control Branch, MS 308, Member AIAA
†Research Engineer, Dynamic Systems and Control Branch, MS 308, Associate Fellow AIAA

I. Introduction

Applying system identification techniques to aircraft flight dynamics problems often involves extracting linear stability and control derivatives from experimental flight test data. These results can then facilitate applications including performance and handling qualities analysis, aircraft redesign, flight simulator development, and control law synthesis. It is important to understand how errors in the data collection and modeling processes manifest in the parameter estimates. This knowledge can improve flight test procedures and instrumentation, thereby saving time and money in the system identification process.

The effects of additive measurement noise, unmodeled dynamics or process noise, and information deficiency due to lack of excitation on system identification results are well understood,[1,2] and a branch of system identification techniques has evolved to consider the effects of using quantized observations.[3,4] In the 1970's, studies[5–8] were conducted to determine the effect of flight instrumentation errors on the aircraft dimensional stability and control derivative estimates using the output-error method in the time domain[1,9] with linear simulation models and doublet inputs. These works focused on time-skews; time lags; sensor position, misalignment, bias, and scale factor errors; and accelerometer and air data boom correction errors. The authors placed a premium on the quality of control input measurements, and also concluded that results varied from aircraft to aircraft. These studies were not able to take advantage of modern control input design and parameter estimation techniques, nor did they consider normalized stability and control derivatives, nor did they examine the effect of sensor resolution, mass and inertia errors, and geometry errors in their studies.

One sector of research and development that could particularly benefit from this information includes the design of subscale, unmanned air vehicles. Although envisioned as cheaper alternatives to manned flight vehicles, these aircraft may become prohibitively expensive due to the cost of high quality on-board sensors that are also small and light weight. Knowing the trade offs between sensor quality and modeling accuracy would allow for better aircraft system solutions. Additionally, mass distribution and aircraft geometry properties are found using intricate computer aided drawing (CAD) models or by experiment. Both are time consuming processes that still have error. Also, unmanned vehicles are often subject to rapid configuration changes or damage from flight testing that change these parameters too rapidly for a CAD analysis. It would therefore benefit designers to have a set of guidelines and recommendations that relate the accuracy of these parameters to the accuracy of dynamic models identified from flight test data.

This paper presents such guidelines. Section II describes a high-fidelity, nonlinear simulation of a transport style aircraft, as well as a system identification maneuver designed for extracting dynamic models. Section III presents the model structure for the aerodynamic force and moment coefficients, as well as the equation-error method for estimating the stability and control derivatives from flight data in the frequency domain. In Section IV, increasing errors are sequentially introduced to each measurement while stability and control derivatives are estimated and recorded within a Monte Carlo analysis. A summarizing table with recommendations to meet 5% and 10% error budgets on the primary stability and control derivatives is presented. This table is the primary contribution of this paper and will give designers guidelines for selecting instrumentation and measurement accuracies. These recommendations are also compared with other flight conditions, parameter estimation methods, and aircraft in this section.

All of the input design, signal processing, and system identification work presented in this paper was done using software written in MATLAB® called System IDentification Programs for AirCraft (SIDPAC),[1] which was developed at NASA Langley Research Center, and is continually expanded and improved. SIDPAC has been applied successfully to a wide variety of flight and wind tunnel experiments at NASA Langley Research Center[1] and elsewhere, and is used at more than 80 institutions worldwide.

II. Materials

A. NASA Generic Transport Model

This work employed a simulation of the NASA Generic Transport Model (GTM), which describes the rigid body flight dynamics of a subscale, transport type aircraft having mass and geometry parameters listed in Table 1. The GTM simulation was selected for analysis because it is a high-fidelity, nonlinear simulation of a subscale aircraft. The GTM was designed to represent a conventional transport type aircraft, having relatively well-known flight dynamics and behaviors. Additionally, the GTM was chosen because a truth model can be extracted from the simulation using finite differences and compared to the Monte Carlo analysis results.

Table 1. Mass and geometry properties of the GTM

Parameter	Variable	Value	Unit
Mass	m	1.5416	slug
Roll Inertia	I_{xx}	1.3270	slug·ft^2
Pitch Inertia	I_{yy}	4.2540	slug·ft^2
Yaw Inertia	I_{zz}	5.4540	slug·ft^2
Coupling Inertia	I_{xz}	0.1200	slug·ft^2
Mean Aerodynamic Chord	$\bar{c}$	0.9153	ft
Wingspan	b	6.8488	ft
Wing Reference Area	S	5.9018	ft^2

The GTM simulates the nonlinear, six degree of freedom, rigid body dynamics of the aircraft. Aerodynamic control surfaces include the elevator, aileron, rudder, spoilers, stabilizers, and flaps. The aerodynamic model used in the GTM is derived from a series of wind tunnel tests conducted at the NASA Langley Research Center.[10] A 5.5% scaled wind tunnel model was tested in the 14 ft by 22 ft subsonic wind tunnel using static and forced oscillation tests to generate an aerodynamic database. That database was augmented with data from rotary balance tests conducted using a 3.5% scaled wind tunnel model in the 20 ft vertical spin tunnel. A polynomial-based aerodynamic model was then extracted from the database using multivariate orthogonal functions, expanded in the aircraft states and controls, and is implemented in the simulation.[1,11,12] The GTM also includes two turbojet engines, the dynamics for which are modeled as a first order lag from the pilot throttle input to the thrust output. This model is based on multivariate orthogonal functions identified from ground testing, with ram drag corrections that vary with altitude and airspeed.

The GTM software is written as MATLAB® code. The user provides an initial state vector and a time history of control surface inputs. The simulation computes time histories of the aircraft translational and rotational positions, velocities, and accelerations, as well as power and thrust states. Additional tools are provided to trim the aircraft and generate linear perturbation models about those trim conditions using central finite differences.

B. Nominal Perturbation Maneuver

Simulation data from a single nominal flight maneuver were examined. For this maneuver, the GTM was trimmed for straight and level flight at a 1200 ft altitude and a 130 ft/s airspeed, which is a typical flight condition for this aircraft.[13] The simulation code determined trim values of +4.52 deg angle of attack, +1.40 deg elevator deflection, and 15% throttle for this condition.

Orthogonal, phase-optimized, multi-sine control input perturbations[1,14] were chosen to excite the GTM for system identification. These multiple-axis inputs are commonly used for system identification at NASA Langley Research Center and have led to good modeling results in a variety of flight conditions including straight and level, hypersonic, high sideslip angles, and post-stall flight.[14,15] Each of the elevator, aileron, and rudder control surface deflections had the form

$$\begin{aligned} \delta(t) &= \delta_0 + \Delta\delta(t) \\ &= \delta_0 + \sum_{k\in K} a_k \sin\left(\frac{2\pi k}{T}t + \phi_k\right) \end{aligned} \tag{1}$$

where δ_0 is the trim value, $\Delta\delta(t)$ is the perturbation, a_k is the amplitude, T is the excitation record length, ϕ_k is the phase angle, $\omega_k = 2\pi k/T$ is the excitation frequency, and K is the set of available frequencies for that input.

The excitation record length was chosen as $T = 35$ s, which corresponds to a fundamental frequency of 0.0286 Hz, to provide enough information content for system identification. Excitation frequencies were selected as integer multiples of this fundamental frequency, between the range 0.2 Hz and 2.0 Hz, where the rigid body dynamics of interest typically reside. Because these frequencies are harmonic multiples, they are mutually orthogonal and were excited simultaneously to shorten experiment durations without correlating

data and deteriorating estimation results. Excitation frequencies were assigned to the inputs in an alternating manner to fully span the bandwidth of the input. For simplicity, amplitudes were selected to have uniform power and normalized such that the elevator, aileron, and rudder have perturbation amplitudes

$$A = a_k\sqrt{M} \tag{2}$$

of 2.0 deg, 0.5 deg, and 1.5 deg, respectively, where M is the number of frequency indices used in the input. These amplitudes are typical of those used in practice;[15] smaller amplitudes result in lower signal-to-noise ratios and larger amplitudes introduce nonlinearities. The phase angles were determined using a simplex search optimization to minimize the relative peak factors

$$\text{RPF} = \frac{\max[\Delta\delta(t)] - \min[\Delta\delta(t)]}{2\sqrt{2}\cdot \text{rms}[\Delta\delta(t)]} \tag{3}$$

of the inputs to keep the aircraft near the trim condition for linear modeling. These excitation inputs are parameterized in Table 2.

The GTM was simulated with these inputs at the reference flight condition and the resulting time history data is shown in Figure 1. Amplitudes of the responses are small enough to use for linear modeling, but large enough to produce good modeling results. Airspeed, air flow angles, and rotational velocity outputs all remain within the region of validity of the aerodynamic database.[10]

III. Methods

A. Aerodynamic Modeling

Observing the conventional simplifying assumptions for a rigid body flight dynamics model of a fixed-wing aircraft,[1,16,17] the nonlinear equations of motion can be rearranged to compute the aerodynamic force and moment coefficients

$$\begin{aligned}
C_Y &= (ma_y)/(\bar{q}S) \\
C_Z &= (ma_z)/(\bar{q}S) \\
C_l &= [I_{xx}\dot{p} - I_{xz}(\dot{r} + pq) + (I_{zz} - I_{yy})qr]/(\bar{q}Sb) \\
C_m &= [I_{yy}\dot{q} + (I_{xx} - I_{zz})pr + I_{xz}(p^2 - r^2)]/(\bar{q}S\bar{c}) \\
C_n &= [I_{zz}\dot{r} - I_{xz}(\dot{p} - qr) + (I_{yy} - I_{xx})pq]/(\bar{q}Sb)
\end{aligned} \tag{4}$$

by substituting measured flight data.[1] The mass, inertia, wing reference area, mean aerodynamic chord, and wingspan of the aircraft are typically known before the flight test. Dynamic pressure, rotational velocities, and translational accelerations are measured by on-board sensors. Rotational accelerations are found by smoothly differentiating angular velocity measurements.[1] The longitudinal coefficient C_X is not included here because it is associated with the slower phugoid mode and is often excluded from a control law design.

The aerodynamic force and moment coefficients in Eq.(4) were modeled in terms of the aircraft states and controls with the linear expansions[1,16,17]

$$\begin{aligned}
C_Y &= C_{Y_\beta}\Delta\beta + C_{Y_p}\frac{b\Delta p}{2V} + C_{Y_r}\frac{b\Delta r}{2V} + C_{Y_{\delta_a}}\Delta\delta_a + C_{Y_{\delta_r}}\Delta\delta_r \\
C_Z &= C_{Z_0} + C_{Z_\alpha}\Delta\alpha + C_{Z_q}\frac{\bar{c}\Delta q}{2V} + C_{Z_{\delta_e}}\Delta\delta_e \\
C_l &= C_{l_\beta}\Delta\beta + C_{l_p}\frac{b\Delta p}{2V} + C_{l_r}\frac{b\Delta r}{2V} + C_{l_{\delta_a}}\Delta\delta_a + C_{l_{\delta_r}}\Delta\delta_r \\
C_m &= C_{m_0} + C_{m_\alpha}\Delta\alpha + C_{m_q}\frac{\bar{c}\Delta q}{2V} + C_{m_{\delta_e}}\Delta\delta_e \\
C_n &= C_{n_\beta}\Delta\beta + C_{Y_p}\frac{b\Delta p}{2V} + C_{n_r}\frac{b\Delta r}{2V} + C_{Y_{\delta_a}}\Delta\delta_a + C_{n_{\delta_r}}\Delta\delta_r
\end{aligned} \tag{5}$$

valid for small deviations about the trim condition, where Δ indicates a perturbation value and the coefficients multiplying the aircraft states and controls are the unknown stability and control derivatives.

Table 2. Multi-sine perturbation input description (record length $T = 35$ s)

Elevator			Aileron			Rudder		
$A = 2.0$ deg $a_k = 0.6667$ deg $M = 22$ RPF $= 1.2445$			$A = 0.5$ deg $a_k = 0.1091$ deg $M = 21$ RPF $= 1.2136$			$A = 1.5$ deg $a_k = 0.3273$ deg $M = 21$ RPF $= 1.0658$		
Index k	Frequency k/T [Hz]	Phase ϕ_k [rad]	Index k	Frequency k/T [Hz]	Phase ϕ_k [rad]	Index k	Frequency k/T [Hz]	Phase ϕ_k [rad]
7	0.2000	3.6221	8	0.2286	3.9280	9	0.2571	5.8733
10	0.2857	4.1272	11	0.3143	6.0649	12	0.3429	4.9406
13	0.3714	3.2037	14	0.4000	0.8306	15	0.4286	3.1968
16	0.4571	2.6584	17	0.4857	1.5477	18	0.5143	0.0323
19	0.5429	0.0811	20	0.5714	2.2952	21	0.6000	3.3582
22	0.6286	2.5869	23	0.6571	1.4435	24	0.6857	4.3454
25	0.7143	6.0820	26	0.7429	6.2755	27	0.7714	3.9451
28	0.8000	0.0769	29	0.8286	3.1900	30	0.8571	5.7802
31	0.8857	1.6735	32	0.9143	0.0810	33	0.9429	4.4729
34	0.9714	1.7690	35	1.0000	2.0319	36	1.0286	3.3028
37	1.0571	0.6256	38	1.0857	3.0491	39	1.1143	0.0384
40	1.1429	5.0289	41	1.1714	3.8835	42	1.2000	3.6866
43	1.2286	2.5389	44	1.2571	2.3799	45	1.2857	4.8036
46	1.3143	5.3888	47	1.3429	1.6406	48	1.3714	0.3270
49	1.4000	0.8353	50	1.4286	5.3963	51	1.4571	0.8943
52	1.4857	0.6303	53	1.5143	2.3521	54	1.5429	1.1219
55	1.5714	2.2350	56	1.6000	5.2871	57	1.6286	5.7885
58	1.6571	2.3720	59	1.6857	1.8165	60	1.7143	3.7299
61	1.7429	0.9076	62	1.7714	1.7858	63	1.8000	5.4749
64	1.8286	5.1943	65	1.8571	0.6440	66	1.8857	2.8322
67	1.9143	1.2656	68	1.9429	5.5245	69	1.9714	3.7967
70	2.0000	3.4607						

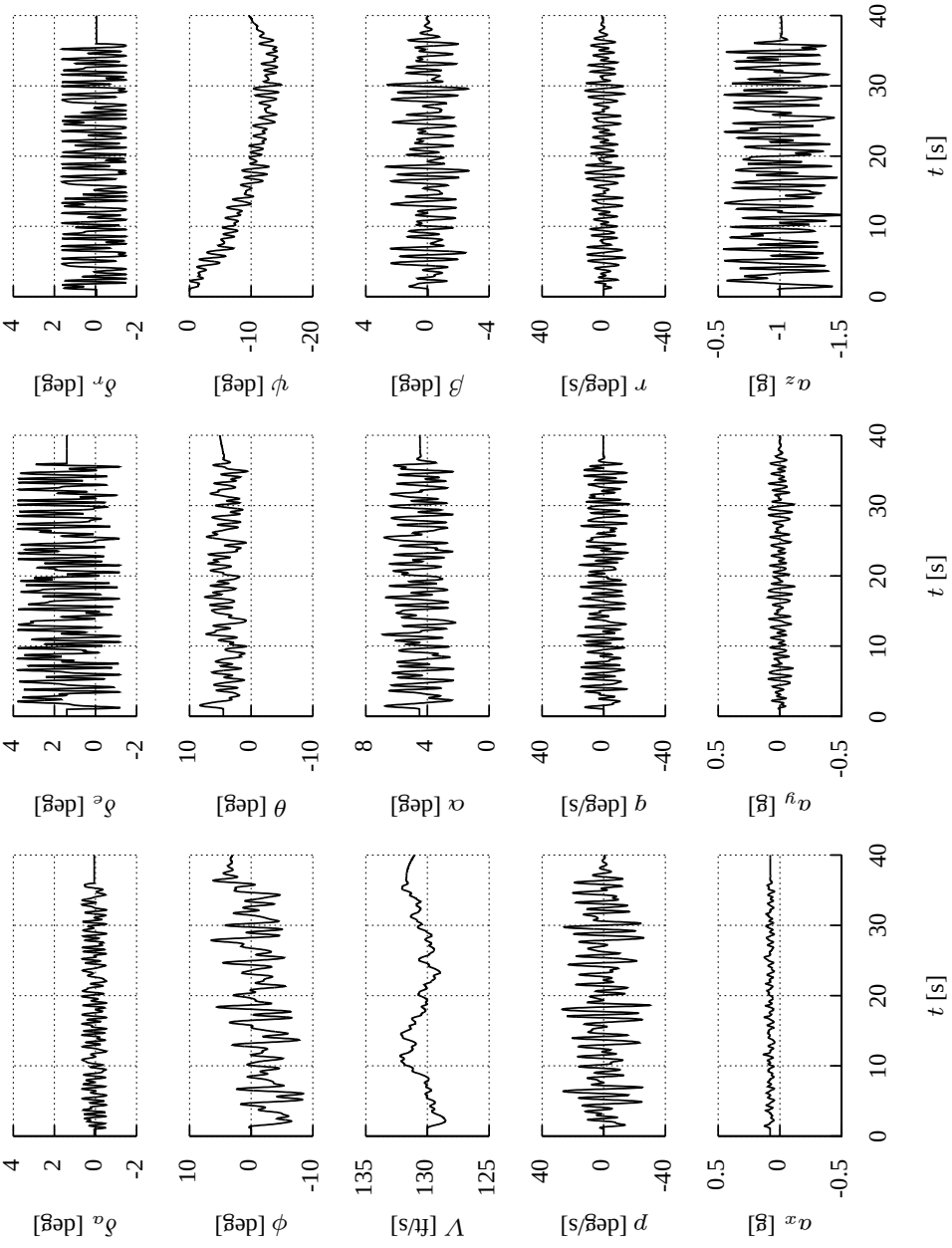

Figure 1. Nominal maneuver simulation data

B. Frequency Domain Equation-Error Parameter Estimation

Given the measurements of the aerodynamic coefficients in Eq.(4) and the model structure in Eq.(5), it is a parameter estimation problem to determine the unknown stability and control derivatives that best match the equations to the data. The equation-error method in the frequency domain[1] was employed to estimate the stability and control derivatives. This method ignores sensor noise and modeling error at higher frequencies, has produced good results in practice, and provides a fast analytical solution amenable to Monte Carlo analysis.

The first step is to transform the data into the frequency domain using the Fourier transform. A measured signal has the finite Fourier transform

$$z(\omega) = \int_0^T z(t) e^{-j\omega t} dt \tag{6}$$

which, for relatively fast sampling frequencies, can be approximated by the discrete Fourier transform

$$z(\omega_m) \simeq \Delta t \sum_{i=0}^{N-1} z(i\Delta t) e^{-j\omega_m i\Delta t} \tag{7}$$

where Δt is the sampling period and N is the number of data samples. A high-accuracy chirp-z transform[1,18] was used to implement the Fourier transform using frequencies between 0.1 Hz and 2.5 Hz, in 0.025 Hz increments.

Each force and moment coefficient in Eq.(5) was arranged into the least-squares framework as

$$\mathbf{z} = \mathbf{X}\boldsymbol{\theta} + \mathbf{e} \tag{8}$$

where $\mathbf{X}$ contains Fourier transforms of the regressor time histories, $\boldsymbol{\theta}$ are the unknown stability and control derivatives, and $\mathbf{e}$ contains the Fourier transform of the error. Minimization of the least-squares cost function

$$J(\boldsymbol{\theta}) = \frac{1}{2}(\mathbf{z} - \mathbf{X}\boldsymbol{\theta})^\dagger (\mathbf{z} - \mathbf{X}\boldsymbol{\theta}) \tag{9}$$

results in the parameter estimates and uncertainty

$$\begin{aligned} \hat{\boldsymbol{\theta}} &= \left[\Re\{\mathbf{X}^\dagger\mathbf{X}\}\right]^{-1} \Re\{\mathbf{X}^\dagger\mathbf{z}\} \\ \boldsymbol{\Sigma}(\hat{\boldsymbol{\theta}}) &= \sigma^2 \left[\Re\{\mathbf{X}^\dagger\mathbf{X}\}\right]^{-1} \end{aligned} \tag{10}$$

where the equation-error variance σ^2 was estimated from the model residuals.[1]

The model fits to the frequency domain force and moment coefficient data using the equation-error method are shown in Figure 2(a). The models fit the data well, as indicated by coefficients of determination above 0.99 and the small residuals shown in Figure 2(b) at one tenth the scale. No unmodeled dynamics are evident within the 2.5 Hz bandwidth. Finite differences were used to interrogate the simulation and determine a truth model for the stability and control derivatives with which to compare the estimation results. Perturbations for the finite differences were selected as the maximum deviations from the trim values in the flight data. The equation-error results were generally within two standard deviations of the true model parameters, further indicating an accurate estimation and that there is sufficient information content in the data for identification. True values and estimates of the stability and control derivatives are listed in Table 3. Differences between the frequency domain equation-error results and the finite differences are due to noise on the measurements, which bias the estimated parameters, as well as modeling error due to linearization and assuming the longitudinal and lateral/directional motions decouple.

IV. Results

The Monte Carlo method was used to evaluate the model accuracy under different measurement errors. In each case, unique Gaussian random noise sequences were used to produce 100:1 signal-to-noise ratios on the surface angle deflection measurements and 20:1 signal-to-noise ratios on the remaining measurements in Figure 1 to make the study more realistic. Afterwards, selected measurements were sequentially and gradually

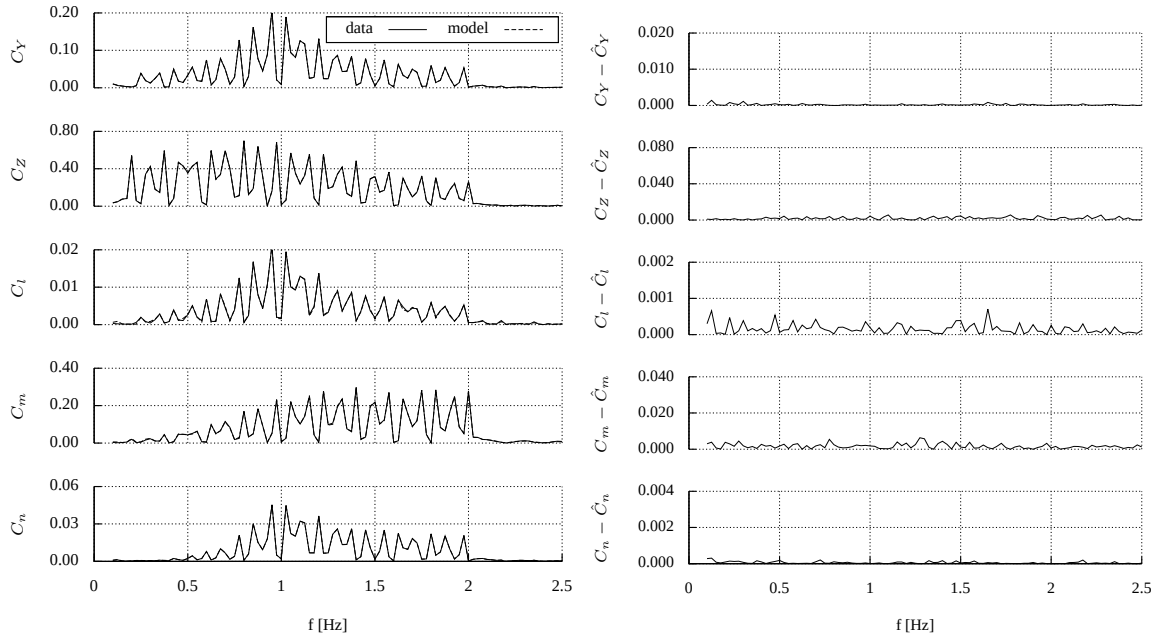

(a) model fits to data

(b) model residuals

Figure 2. Model fits to the nominal flight data using the equation-error method in the frequency domain

Table 3. Stability and control derivatives and nominal estimates for the GTM

Derivative	Numerical Central Finite Difference θ	Frequency Domain Equation-Error $\hat{\theta} \pm \hat{\sigma}(\hat{\theta})$
C_{Y_β}	-1.0125	-1.0065 ± 0.0037
C_{Y_p}	$+0.0543$	$+0.0735 \pm 0.0158$
C_{Y_r}	$+0.8574$	$+0.8877 \pm 0.0238$
$C_{Y_{\delta_a}}$	-0.0177	-0.0155 ± 0.0032
$C_{Y_{\delta_r}}$	$+0.3387$	$+0.3390 \pm 0.0012$
C_{Z_α}	-4.8370	-4.8345 ± 0.0077
C_{Z_q}	-27.102	-27.609 ± 0.5040
$C_{Z_{\delta_e}}$	-0.4807	-0.4801 ± 0.0093
C_{l_β}	-0.1432	-0.1393 ± 0.0029
C_{l_p}	-0.3542	-0.3333 ± 0.0123
C_{l_r}	$+0.1331$	$+0.1535 \pm 0.0186$
$C_{l_{\delta_a}}$	-0.0760	-0.0735 ± 0.0025
$C_{l_{\delta_r}}$	$+0.0290$	$+0.0293 \pm 0.0009$
C_{m_α}	-1.6349	-1.6134 ± 0.0068
C_{m_q}	-41.215	-41.292 ± 0.4441
$C_{m_{\delta_e}}$	-1.7744	-1.7924 ± 0.0082
C_{n_β}	$+0.2165$	$+0.2147 \pm 0.0009$
C_{n_p}	-0.0408	-0.0461 ± 0.0039
C_{n_r}	-0.3840	-0.3892 ± 0.0059
$C_{n_{\delta_a}}$	-0.0025	-0.0032 ± 0.0008
$C_{n_{\delta_r}}$	-0.1691	-0.1692 ± 0.0003

deteriorated to various levels, as discussed later, and parameter estimation results of the stability and control derivatives were recorded. To assure that results had converged, one thousand runs were performed for each measurement selected and for each level of deterioration.

Figures were generated for only the primary, on-axis stability and control derivatives. The secondary, off-axis derivatives are generally less important for performance analysis and control synthesis, and their estimates diverged more quickly with measurement degradation. Each plot marker represents the mean value of one thousand different estimates. The error bars represent the two-standard-deviation spread of those results. The dashed lines show the ±10% bounds of the finite difference values. When the two-standard-deviation bars extend past the error bounds of the finite difference values, that derivative no longer meets that error criteria. A table of recommendations is presented in Section V to summarize these results. A more detailed description of the results of this study is forthcoming in a technical memorandum.

A. Sensor Measurement Resolution

Sensor measurements were degraded by quantizing the noisy measurements to various degrees before using the data in the parameter estimation process. This mimics manufacturer sensor resolutions and the analog-to-digital conversion process that occurs in flight hardware. As an example, Figure 3(a) shows the angle of attack and side slip angle time histories of the nominal data set with added noise. Figure 3(b) then shows these time histories quantized with a resolution of 0.6 degrees. Depending on the random noise sequence and the quantization level, the measurement can take on different values than the original time series, which impacts the parameter estimation. After all the measurements had noise added and a particular set of measurements were quantized, stability and control derivatives were estimated and results were recorded.

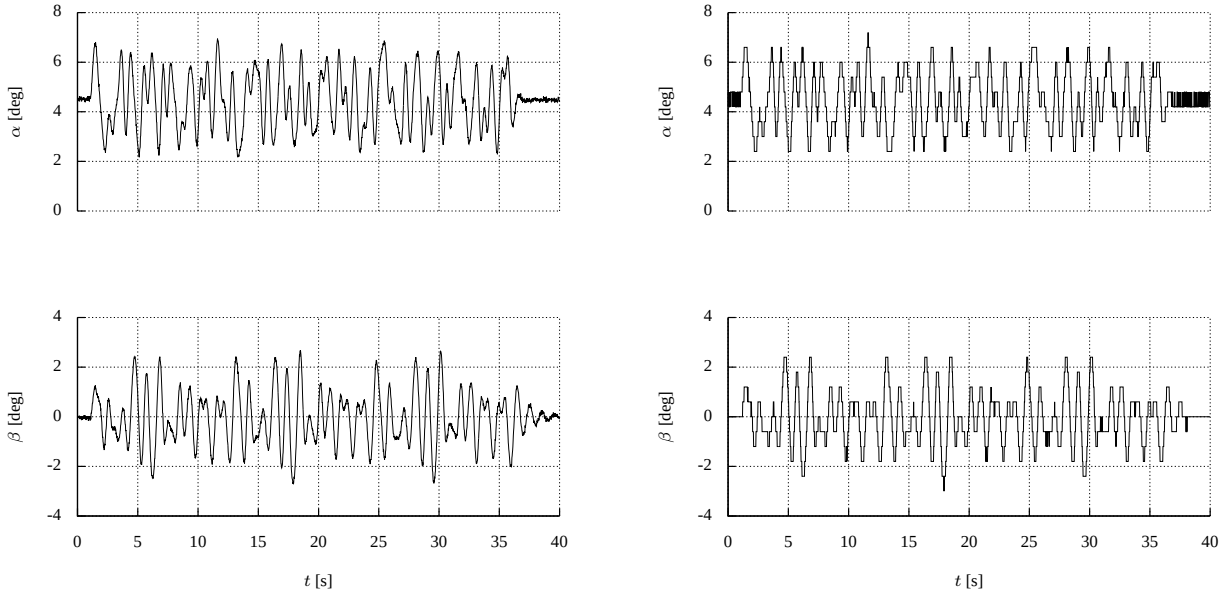

(a) nominal measurements with added noise

(b) measurements quantized at 0.6 deg

Figure 3. Quantized air flow measurements example

Figure 4 shows, for example, the primary stability and control derivatives estimated for various levels of quantization on the air flow angle measurements. At full resolution with no quantization error, the nominal estimation case presented in Figure 2 and Table 3 is recovered.

As the quantization becomes coarser, stability and control derivative estimates increase only slightly in variance. This is because the noise on the measurements is small compared to the magnitude of the signals in the frequency region where the estimation occurs. The bias, however, increases significantly with measurement error and causes the estimates to diverge from the true solutions, as seen in Figure 4. The lateral/directional dynamics typically diverge faster than the longitudinal dynamics because there are more parameters to estimate and more information is consequently needed to achieve good estimates. As the

degradation progresses, the damping derivatives generally diverge first, followed by the control derivatives, and then the static derivatives. Damping derivatives are typically difficult to accurately estimate in practice, as indicated by the order of magnitude larger error bounds in Table 3. The control derivatives are usually estimated well because system identification requires good control surface excitation. Finally, static derivatives are usually well-estimated because they are strong parameters that tend to dominate the flight dynamic responses. The off-axis parameters, such as $C_{n_{\delta_a}}$, are not shown because they are generally smaller in value and lesser in importance than the on-axis derivatives, such as $C_{n_{\delta_r}}$. These parameters also tend to diverge quicker with degrading measurement resolutions.

Several other measurement sources were degraded in addition to air flow angle sensors. Among them were gyroscopes, which measure the rotational velocities p, q, r that appear in Eq.(4) and (5). Linear accelerometers measure the translational accelerations a_y and a_z, which only affect the side force C_Y and heave force C_Z coefficients. The control surface deflection angles δ_e, δ_a, δ_r are measured using potentiometers. The dynamic pressure is measured using a Pitot-static tube, and then the airspeed is calculated using

$$V = \sqrt{2\bar{q}/\rho} \tag{11}$$

where the air density ρ is found using a standard atmosphere table. Errors were not introduced into the Euler angle solutions or the GPS position measurements because these do not appear in Eq.(4).

Additionally, a method has recently been developed for reconstructing air flow angle measurements from gyroscopes and Euler angle measurements (which can also be reconstructed if not available).[19] For small perturbations about a trim condition at a low angle of attack, the differential equations

$$\begin{aligned} \dot{\alpha} &\simeq q - \beta p + (\cos\phi\cos\theta + a_z)/V \\ \dot{\beta} &\simeq \alpha p - r + (\sin\phi\cos\theta + a_y)/V \end{aligned} \tag{12}$$

can be integrated from initial conditions using flight data measurements to reconstruct angle of attack and sideslip angle. By reconstructing these time series, fewer sensors are needed, which reduces weight, complexity, and calibration times. Stability and control derivatives were also estimated while reconstructing angle of attack and sideslip angle using degraded gyroscope and accelerometer measurements.

B. Mass Properties and Aircraft Geometry

Measurements of the mass distribution and aircraft geometry were degraded by adding a uniformly distributed, random bias to each of the mass and geometry properties. This type of error results from incorrect knowledge of the aircraft properties. In the case of the mass distribution, random biases were simultaneously added to the mass m and the inertias I_{xx}, I_{yy}, I_{zz}, and I_{xz}, and then parameter estimation was performed. Typically these measurements are performed on the ground, before flight test data collection, using drafting software or experimental swinging techniques. Errors develop due to low fidelity modeling; inaccuracies in measuring sub-component mass, inertia, and geometry; and systematic errors in conducting the swing tests. These parameters affect the nondimensionalization of the aerodynamic force and moment coefficients. The impact of errors on the mass distribution, for example, are shown in Figure 5. With no error, the stability and control derivative estimates are very close to the true values from the finite differences. As the measurement degrades, the mean estimates remain approximately the same, but the variation increases. The effect of the product of inertia I_{xz} was also examined. This parameter is time consuming to find experimentally because the test model has to be mounted at an angle and then swung. As measurements get progressively worse, the product of inertia becomes more important; for better measurements, I_{xz} may be safely ignored without much effect on the parameter estimates.

Measurements of the aircraft geometry, described by the mean aerodynamic chord $\bar{c}$, the wingspan b, and the wing area S, were simultaneously degraded while estimating stability and control derivatives. These values typically come from measurements or drafting software computations, and appear in the nondimensionalization of the force and moment coefficients as well as in the aerodynamic model regressors. The resulting parameter estimation errors follow the same trend as those for the mass distribution variation.

C. Comparisons

The results discussed in the previous two sections were for one aircraft flying at one trim condition and using one method of parameter estimation. To begin to understand how such factors may influence the parameter

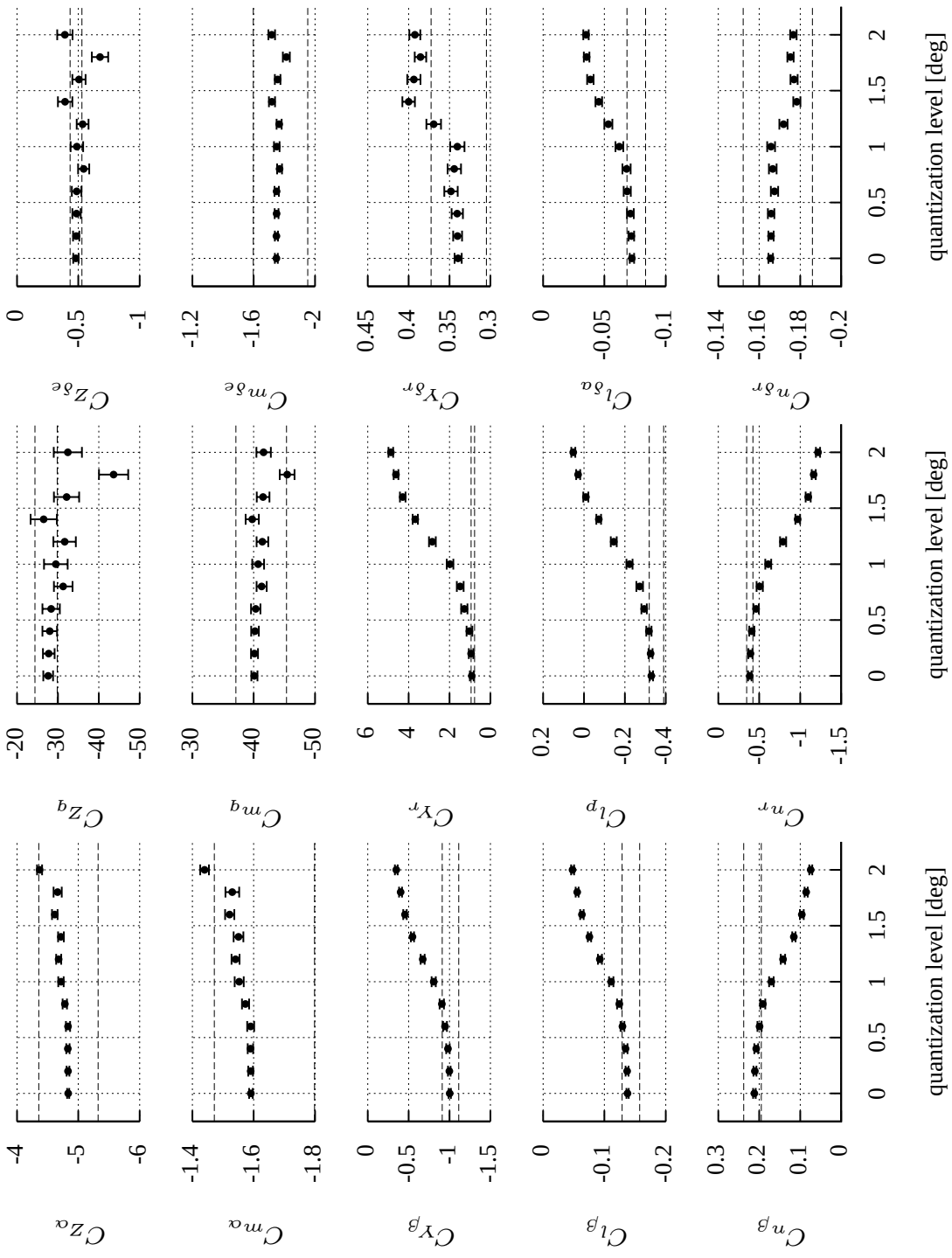

Figure 4. Variation of stability and control derivatives with air flow angle resolution

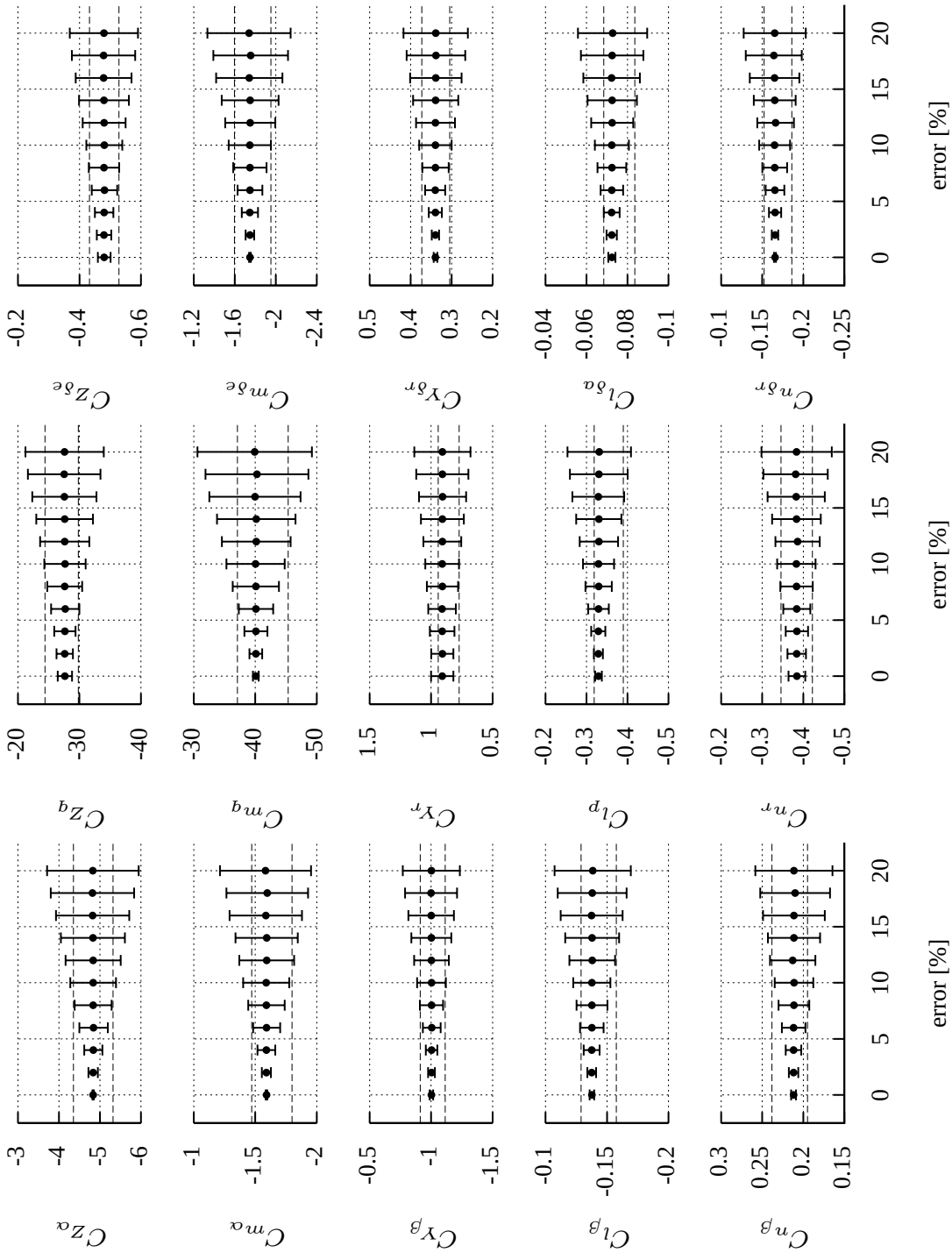

Figure 5. Variation of stability and control derivatives with mass and inertia accuracy

estimation error trends, the analysis was first repeated for different trim conditions. Figure 6 shows the pitching moment stability and control derivatives under degrading gyroscope measurements for trim angles of attack between 0 deg and 10 degrees. The GTM was not trimmed at or above stall in this analysis, but such flight conditions may be considered in the future. Although the numerical values of the stability and control derivatives change with varying trim conditions, the character of the estimate divergence does not and the supplied recommendations remain consistent.

The equation-error method in the frequency domain was also changed to the equation-error method in the time domain to reveal how sensitive the recommendation results are to the parameter estimation technique. This was done using the same general approach, but using time-domain data directly, instead of first transforming the time-domain data into the frequency domain. Analysis in the time domain introduced larger biases into the stability and control estimates and caused them to diverge faster than the corresponding frequency domain estimates. This can be seen, for instance, by comparing the gyroscope degradation results at the nominal trim condition in Figure 7 to the corresponding results in Figure 6. Recall that the nominal angle of attack is 4.52 degrees. For example, the pitch damping C_{m_q} exceeds 10% bounds at about 6 deg/s resolution when using the frequency domain analysis, but at only 4 deg/s resolution when using the time domain analysis. Other parameters, such as C_{Y_r} and C_{l_p} do not fall within the 10% bounds even with no measurement deterioration. Unmodeled dynamics, such as sensor noise, quantization error, and quantization chatter, create these biases in the time domain analysis. The frequency domain analysis is more robust to these types of error since only the low frequency data up to 2.5 Hz are considered. Therefore, the supplied recommendations for measurements accuracies may be overly optimistic if a time domain equation-error method is used. Output-error in the time domain is another parameter estimation technique that will be considered in the future and compared with previous results.

The analysis was also applied to the nonlinear F-16 simulation[1,20] supplied in SIDPAC to begin to understand how the recommendations scale with aircraft size. The F-16 was trimmed for straight and level flight at a 10,000 ft altitude and with a 450 ft/s airspeed and 5 deg angle of attack, which represents a typical flight condition. Although the GTM and the F-16 have different mass properties, stability and control derivative estimation results with degrading measurements showed similar trends and consistent accuracy recommendations. Previous studies[5,7] reported differently, but this is expected to be caused by the use of dimensional derivatives which do not take into account vehicle size and mass properties. Therefore, results are more robust to vehicle size when using normalized stability and control derivatives.

V. Conclusions

Errors in sensor measurements, mass properties, and aircraft geometry are important factors that impact the identification of stability and control derivatives for applications including performance analysis, flight simulator development, and control synthesis. One particular application concerns small and low cost unmanned air vehicles, where it is desired to have good modeling results using inexpensive hardware.

This paper investigated these dependencies using a nonlinear simulation of a subscale transport type aircraft. A system identification maneuver was designed to excite all axes of the aircraft dynamic response using orthogonal phase-optimized multi-sines. After a model structure was chosen, parameter estimation was performed in the frequency domain using the equation-error method. Parameter estimation in this nominal case had low errors and matched the data well, indicating an appropriate model structure and that there was enough information content in the data. This process was repeated for various states of measurement deterioration.

The primary contribution of this paper is Table 4, which recommends minimum measurement accuracy budgets for meeting 5% and 10% error margins on the stability and control derivative estimates. These recommendations were obtained by progressively degrading sensor measurements, one at a time, and observing how the estimates change within a Monte Carlo analysis. Thus, exceeding the recommendation in a single measurement produces estimates likely to exceed the accuracy tolerance. In practice, a 10% error margin on the stability and control derivatives is usually sufficient. These recommendations can be used as guidelines for flight test specification and design, and for flight test planning and execution. Additional findings can be enumerated as the following:

1. Accurate estimates of stability and control derivatives can be obtained by reconstructing angle of attack and sideslip angle measurements from gyroscopes and accelerometers; however, to do so, these sensors require at least a three-fold increase in resolution. Nonetheless, this method appears to be a viable

alternative to using air flow angle vanes for system identification, as these sensors disturb the local flow, add complexity to the aircraft, and are difficult to calibrate.

2. The product of inertia I_{xz} was found to have a small impact on stability and control derivative estimates if other mass distribution measurements were accurate. This term may therefore be safely ignored to save time and money if aircraft mass distributions are being determined experimentally. Although not difficult in a CAD analysis, experimentally determining this product of inertia is time consuming.

3. Repeated analysis showed that the results listed in Table 4 were not sensitive to the trim conditions below stall. Trim conditions at and above stall were not yet attempted because for transport style aircraft, these represent somewhat unusual flight conditions.

4. Equation-error in the frequency domain used less computation time and was more accurate in estimating stability and control derivatives than equation-error in the time domain. This is because there are fewer data points to use in the frequency domain, which are also more accurate and are not sensitive to the high frequency chatter that occurs from quantization.

5. Results in Table 4 were found to scale to full size aircraft, per analysis using the F-16 nonlinear simulation. This is due to the fact that the effect of most of the varying parameters is taken into account through nondimensionalizing the stability and control derivatives.

Table 4. Recommended measurement accuracies for achieving specific error budgets

Measurement	Variable	5% Error	10% Error	Unit
Air Flow Angles	α, β	0.4	0.5	deg
Dynamic Pressure	$\bar{q}$	6.0	7.0	lbf/ft^2
Gyroscopes	p, q, r	4.0	6.0	deg/s
Gyroscopes[a]	p, q, r	1.0	2.0	deg/s
Accelerometers	a_x, a_y, a_z	0.04	0.10	g
Accelerometers[a]	a_x, a_y, a_z	0.04	0.05	g
Potentiometers	δ_e, δ_a, δ_r	0.4	0.5	deg
Mass and Inertia	m, I_{xx}, I_{yy}, I_{zz}, I_{xz}	4.0	8.0	%
Mass and Inertia[b]	m, I_{xx}, I_{yy}, I_{zz}	4.0	6.0	%
Aircraft Geometry	$\bar{c}$, b, S	2.0	5.0	%

[a]while reconstructing α and β[19]
[b]while neglecting I_{xz}

A more detailed description of these results will be submitted as a technical report. Plots from each case will be included. Additionally, other aircraft, measurements errors, parameter estimation techniques, and trim conditions may be investigated.

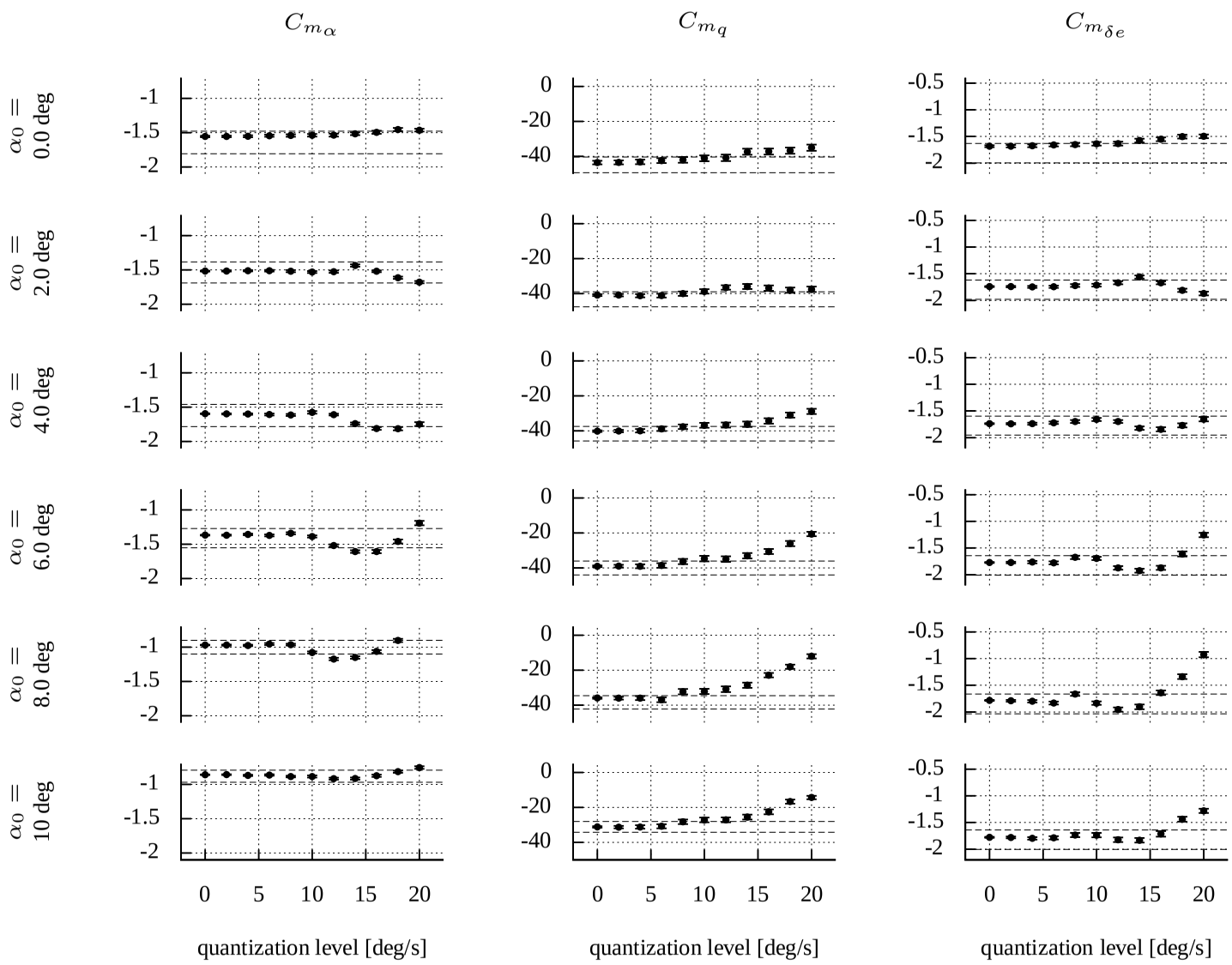

Figure 6. Variation of pitching moment derivatives with varying gyroscope resolution for several trim conditions

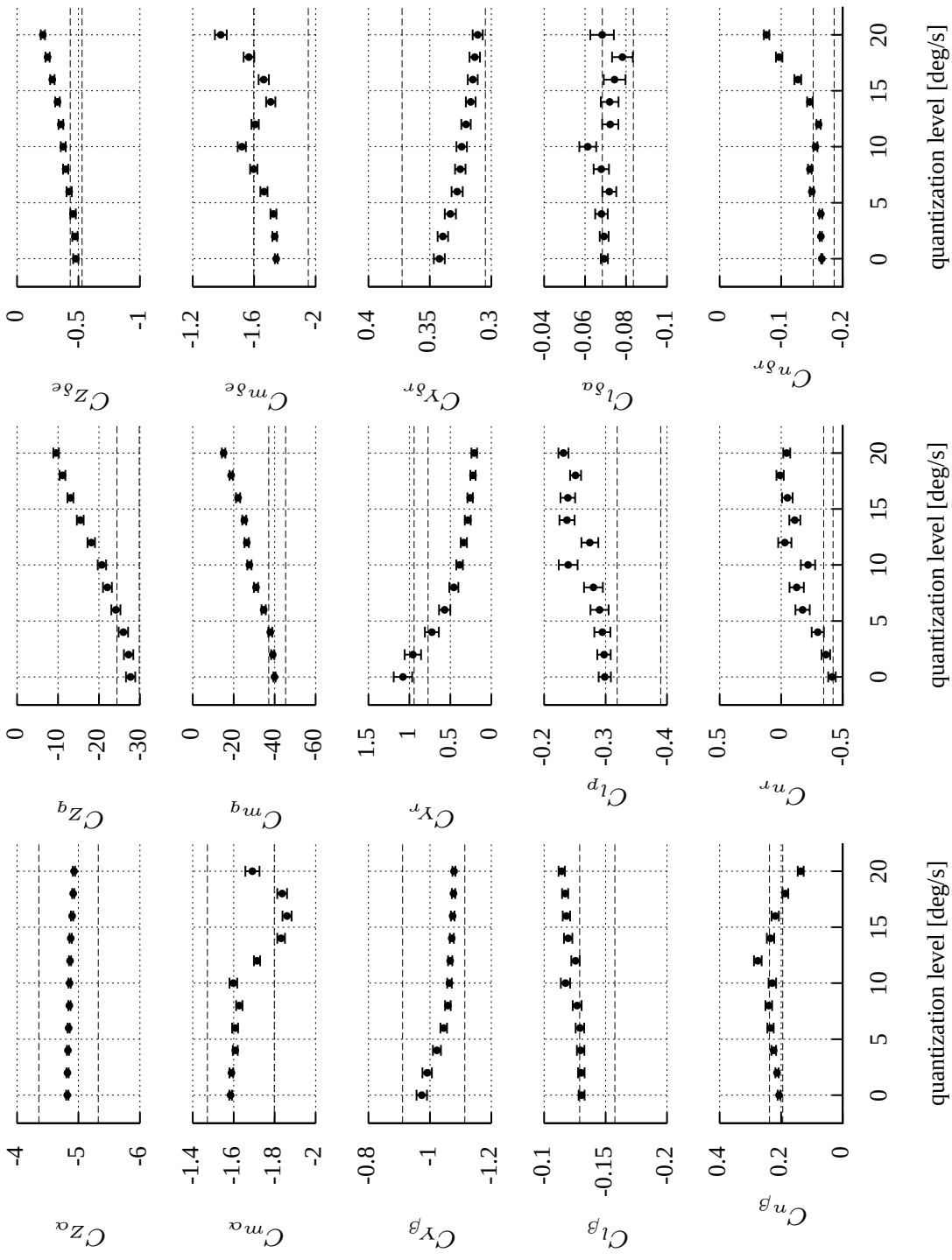

Figure 7. Variation in stability and control derivatives with gyroscope resolution using equation-error parameter estimation in the time domain

References

[1]Klein, V. and Morelli, E., *Aircraft System Identification: Theory and Practice*, AIAA Education Series, AIAA, 2006.

[2]Ljung, L., *System Identification: Theory for the User*, Information and System Sciences Series, Prentice Hall, Upper Saddle River, NJ, 2nd ed., 1999.

[3]Wang, L., Yin, G., Zhang, J., and Zhao, Y., *System Identification with Quantized Observations*, Springer, 2010.

[4]Konishi, K. and Kato, H., "A System Identification Method With Roughly Quantized Data Using Semidefinite Programming," Industrial Electronics Conference, IEEE, 2009, pp. 1426–1431.

[5]Sorenson, J., "Analysis of Instrument Error Effects on the Identification Accuracy of Aircraft Parameters," Tech. Rep. CR-112121, NASA, Washington D.C., May 1972.

[6]Steers, S. and Illiff, K., "Effects of Time-Shifted Data on Flight-Determined Stability and Control Derivatives," Tech. Rep. TN-D-7830, NASA, Washington D.C., March 1975.

[7]Hodge, W. and Bryant, W., "Monte Carlo Analysis of Innacuracies in Estimated Aircraft Parameters Caused by Unmodeled Flight Instrumentation Errors," Tech. Rep. TN-D-7712, NASA, Washington D.C., February 1975.

[8]Sorenson, J., Mohr, R., and Cline, T., "Instrumentation Requirements for Aircraft Parameter Identification With Application to the Helicopter," Tech. Rep. CR-132675, NASA, Washington D.C., June 1975.

[9]Maine, R. and Iliff, K., "Application of Parameter Estimation to Aircraft Stability and Control: The Output-Error Approach," Tech. Rep. Reference Publication 1168, NASA, June 1986.

[10]Murch, A. and Foster, J., "Recent NASA Research on Aerodynamic Modeling of Post-Stall and Spin Dynamics of Large Transport Aircraft," No. 2007–463 in 45th AIAA Aerospace Sciences Meeting and Exhibit, AIAA, Reno, NV, January 2007.

[11]Morelli, E., "Global Nonlinear Aerodynamic Modeling using Multivariate Orthogonal Functions," *Journal of Aircraft*, Vol. 32, No. 2, March–April 1995, pp. 270–277.

[12]Morelli, E. and DeLoach, R., "Wind Tunnel Database Development using Modern Experiment Design and Multivariate Orthgonal Functions," No. 2003–653 in 41st AIAA Aerospace Sciences Meeting and Exhibit, AIAA, Reno, NV, January 2003.

[13]T. Jordan, J. Foster, R. B. and Belcastro, C., "AirSTAR: a UAV Platform for Flight Dynamics Control System Testing," No. AIAA-2006-3307 in Aerodynamic Measurement Technology and Ground Testing Conference, AIAA, San Francisco, CA, June 2006.

[14]Morelli, E., "Flight-Test Experiment Design for Characterizing Stability and Control of Hypersonic Vehicles," *Journal of Guidance, Control, and Dynamics*, Vol. 32, No. 3, May–June 2009, pp. 949–959.

[15]Morelli, E., "Flight Test Maneuvers for Efficient Aerodynamic Modeling," No. 2011–6672 in AIAA Atmospheric Flight Mechanics Conference, AIAA, Portland, OR, August 2011.

[16]McRuer, D., Ashkenas, I., and Graham, D., *Aircraft Dynamics and Automatic Control*, Princeton Universtiy Press, 1973.

[17]Stevens, B. and Lewis, F., *Aircraft Control and Simulation*, Wiley, 2003.

[18]Morelli, E., "High Accuracy Evaluation of the Finite Fourier Transform Using Sampled Data," Tech. Rep. TM 110340, NASA, Hampton, VA, June 1997.

[19]Morelli, E., "Real-Time Aerodynamic Parameter Estimation without Air Flow Angle Measurements," No. 2010–951 in AIAA Flight Mechanics Conference, AIAA, Toronto, Ontario, August 2010.

[20]Nguyen, L., Ogburn, M., Gilbert, W., Kibler, K., Brown, P., and Deal, P., "Simulation Study of Stall/Post-Stall Characteristics of a Fighter Airplane with Relaxed Longitudinal Static Stability," Technical Report TP 1538, NASA, 1979.